Weather and Climate Extremes 39 (2023) 100530

Contents lists available at ScienceDirect

Weather and Climate Extremes

journal homepage: www.elsevier.com/locate/wace

Recent changes in circulation patterns and their opposing impact on extreme precipitation at the west coast of Norway

Karianne Ødemark [a,b,*], Malte Müller [a,b], Cyril Palerme [a], Ole Einar Tveito [a]

[a] Norwegian Meteorological Institute, Oslo, Norway
[b] Department of Geosciences, University of Oslo, Norway

ARTICLE INFO

Keywords:
Extreme precipitation
Circulation patterns
Ensemble data set
Trends

ABSTRACT

Understanding recent and future changes of extreme precipitation is essential for climate change adaptation. Here, we use 3800 extreme precipitation events produced by an ensemble seasonal prediction system. The ensemble represents the climate from 1981 to 2018 and we analyse 3-day maximum precipitation events in September–October–November for the west coast of Norway. Two dominant atmospheric patterns, described by an empirical orthogonal function (EOF) analysis, are related to the results of the extreme value statistics. The principal components of the second and third mode of EOFs have significant trends over the last 40 years, but with an opposing impact on the return values of extreme precipitation. This explains the observed stationarity of extreme precipitation over recent decades at the west coast of Norway, which was also found in previous studies. The second mode of EOFs also shows a relation to the sea-ice coverage in the Barents and Kara Seas, which suggests a connection between the decline of sea-ice to the changes in the atmospheric pattern.

1. Introduction

Extreme precipitation events can lead to excess surface water and floods and are becoming an amplifying societal cost as a result of urbanization and our warming climate. A warmer climate will lead to an increase in the intensity (Boucher et al., 2013; Kharin et al., 2013; Fischer and Knutti, 2016) as well as the frequency (Fischer and Knutti, 2016; Papalexiou and Montanari, 2019) of the heaviest precipitation events. For example, for each additional degree Celcius of the global temperature, the most intense precipitation events which are observed today will likely occur twice as often (Myhre et al., 2019). Detailed knowledge about extreme precipitation events is important for advanced predictions on weather-to-climate time scales. When determining the climatic estimates which critical infrastructures are designed after, it is crucial to understand potential risks caused by extreme weather, so the constructions will endure the strain caused by current and future climate.

For statistical analysis of extreme precipitation events long time series are required, which is a major challenge when using observational or reanalysis data. Kelder et al. (2020) have demonstrated how an ensemble hindcast data set from a seasonal prediction system can be utilized to retrieve a large number of plausible weather event realizations. In their case, a 3800 year long data set was constructed to study extreme precipitation in the period from 1981 to 2018. They showed that by using this large ensemble the confidence intervals for the extreme value distribution are considerably smaller than by using data from a reanalysis only. Hence, the increased number of events by a factor of 100, provides the opportunity to significantly reduce uncertainties in the statistical analysis, and in turn, to improve design values, especially for values with high return periods.

In addition, these large ensemble data sets give us the opportunity to investigate different physical drivers for high impact weather events and can potentially improve our understanding of the relation between extreme precipitation with other dynamical components in the coupled Earth's system, such as atmospheric weather patterns, sea-ice variability, or land- and ocean-surface conditions.

Precipitation in Norway is to a large extent dominated by the large-scale atmospheric circulation (Azad and Sorteberg, 2017) which in turn is driven by the Earth's energy balance through complex processes. There has been tremendous effort on understanding connections between atmospheric circulation and various drivers of the coupled Earth's system (Vihma, 2014; Bintanja et al., 2020). The poleward shift in the North Atlantic storm track can through deviations in strength and location of cyclones lead to changes in regional climate (Wickström et al., 2020). There is still no consensus of the dominant mechanism causing the shift, and several mechanisms may act in parallel (Tamarin-Brodsky and Kaspi, 2017). Reductions of sea-ice and snow cover is a part of a complex climate system feedback, that together with

* Corresponding author at: Norwegian Meteorological Institute, Oslo, Norway.
E-mail address: karianneo@met.no (K. Ødemark).

https://doi.org/10.1016/j.wace.2022.100530
Received 16 November 2021; Received in revised form 9 November 2022; Accepted 18 November 2022
Available online 23 November 2022

changes in atmospheric and ocean circulation can change the energy balance (Serreze and Barry, 2011). Several studies connect changes in mid-latitude weather to changes in atmospheric circulation caused by the decreasing sea-ice coverage in the Arctic (Screen, 2017; Kolstad and Screen, 2019). The changes in atmospheric circulation seen is found to be dependent on the geographical region of sea-ice loss. Specifically, Sun et al. (2015) found that sea ice loss in the Atlantic sector caused a weakening of the upper-level westerly winds, whereas sea ice loss in the Pacific sector caused a strengthening. Other studies highlight ocean variability as an important mechanism (Sato et al., 2014; Tokinaga et al., 2017). Some skepticism about the importance of sea-ice in driving mid-latitude weather extremes has been expressed (Blackport et al., 2019), however, the comprehensive study performed in the Polar Amplification Model Intercomparison Project's (PAMIP) (Smith et al., 2019) contribution to the sixth Coupled Model Intercomparison Project (CMIP6) (Eyring et al., 2016) find that simulations from 16 models show a weakening of mid-latitude tropospheric westerly winds in response to projected Arctic sea ice loss (Smith et al., 2022). The modelled response is robust among the models, but the response is weak relative to inter-annual variability.

Weather regimes favourable for precipitation extremes in the North Atlantic Region are dominated by negative geopotential height anomalies that enhances extratropical cyclone activity as described in Pasquier et al. (2019). These regimes are associated with higher than normal frequencies of Atmospheric Rivers (ARs), which are narrow filaments of high water vapour transport. More than 90% of the meridional water vapour transport in midlatitudes is located in these narrow, elongated regions related to warm conveyor belts within the warm sector of extratropical cyclones (Zhu and Newell, 1998) . While being responsible for the majority of water vapour transport polewards, ARs cover less than 10% of the area of the globe (Gimeno et al., 2014). They transport water at volumetric flow rates similar to those of the world's largest rivers. Landfalling atmospheric rivers cause heavy rainfall and potentially flooding, especially where the flow of moist air is lifted orographically in areas with steep topography. In the past decades, the awareness of landfalling ARs and their association with extreme precipitation in Norway has increased dramatically. Stohl et al. (2008) and Sodemann and Stohl (2013) provide evidence for the important connection between moisture transport and high impact Norwegian weather. Stohl et al. (2008) show that the extreme weather event "Kristin" in September 2005 was indeed an atmospheric river with a large flux of warm moist air detectable across the North Atlantic. When impinging upon the mountainous area in southwest Norway the AR created an extreme precipitation event followed by flooding and landslides and caused a considerable infrastructure damage and loss of human life. While Stohl et al. (2008) described one particular event, Benedict et al. (2019) found that more than 85% of extreme precipitation events on the west coast of Norway during the cold season are connected to ARs. However, extreme precipitation amounts are not linearly linked to the strength and intensity of the AR, but local conditions are important factors influencing precipitation amounts (Ødemark et al., 2020; Michel et al., 2021). The southern west coast of Norway is the wettest region in the country, where the annual precipitation can exceed 3000 mm. The annual precipitation in this region shows an increasing trend (Kuya et al., 2021). However, there are inter-seasonal variations. For the fall season, which is the focus in the present study, no trend is found. Further, Kelder et al. (2020) analysed variability in precipitation in autumn at the west coast of Norway and found no trend in extreme precipitation for this period.

A critical factor determining the intensity of precipitation is the flow direction of the moisture transport, as it is most efficient when hitting the mountain range at an perpendicular angle (Michel et al., 2021). The complex terrain on the Norwegian coast is characterized by intricate fjords adjacent to steep mountains, which can give rise to very local weather and climate conditions due to the direction of the moisture flow (Ødemark et al., 2020), which in turn is controlled by the large-scale atmospheric circulation. Michel et al. (2021) give a broad overview of the characteristics of the atmospheric environment during extreme precipitation events in Norway, with both regional and seasonal aspects. This study investigates how dominant long-term and large-scale atmospheric patterns relate to extreme precipitation events in Norway. Several studies have examined the connection between the probability of extreme events to changes in atmospheric circulation (Francis and Vavrus, 2012; Coumou et al., 2014; Horton et al., 2015). An increase in the occurrence or persistence of high-amplitude wave patterns is expected to alter the likelihood of extreme events. Francis and Vavrus (2012) describes how a slower progression of upper-level waves associated with Arctic amplification would cause mid-latitude weather patterns to be more persistent, which may lead to an increased probability of extreme weather events, such as drought, flooding, cold spells, and heat waves.

A special emphasis in this study is to investigate whether there are dominant long-term atmospheric weather patterns that are conducive for extreme precipitation events, and further whether there are changes in these patterns over time. In the present study, a sample of 3800 extreme precipitation events, following the method in Kelder et al. (2020), and the related mean seasonal atmospheric states obtained from a hindcast data set of a seasonal forecasting system is analysed. This gives us the opportunity to study the interconnections and changes of the occurrence of extreme precipitation with dominant seasonal atmospheric weather patterns over the last 40 years. In the following section the SEAS5 seasonal prediction system (Johnson et al., 2019) and the method for constructing the combined data set are described in more detail together with the method for analysing dominant long term atmospheric patterns. In Section 3 we elaborate on the results and a discussion and conclusions follow in Section 4.

2. Data and method

In this study we utilize a 25 member ensemble hindcast data set of the European Centre for Medium-Range Weather Forecast's (ECMWF's) seasonal prediction system SEAS5. SEAS5 is a coupled atmosphere–ice–ocean model with a horizontal resolution of around 35 km. SEAS5's atmospheric component is based on cycle 43r1 of the ECMWF-Integrated Forecasting System (IFS) (ECMWF, 2016). The spectral horizontal resolution is T319 and there are 91 vertical layers. The NEMO ocean model (Nucleus for European Modelling of the Ocean, Madec et al. (2017)) and LIM2 sea-ice model (Louvian-la-Neuve Sea Ice Model, Fichefet and Maqueda (1997)) are coupled to the atmospheric system, and have a horizontal resolution of 0.25-degrees. The atmospheric and ocean-ice model systems are initialized by the ERA-Interim (Dee et al., 2011) and OCEAN5 reanalysis (Zuo et al., 2018), respectively.

The ensemble members are generated from perturbations to the ocean and atmosphere initial conditions and from stochastic model perturbations. The SEAS5 hindcast consists of 25 members initiated monthly, and each member spans over 7 months for the years 1981 to present. In this study we use the hindcast data from 1981 to 2018.

The members of individual ensemble forecasts need to be independent for the statistical analysis of extreme precipitation. Because of the chaotic nature of the atmospheric system, we assume that precipitation events are not predictable more than a few weeks in advance and, thus, the first month of the model run is discarded to avoid dependent events. It can be argued that due to the slowly varying components of the atmosphere–ocean system, extreme precipitation events might cluster beyond the discarded first month of the model run. However, Kelder et al. (2020) showed that when removing the first month of the ensemble members they can be considered to represent independent extreme precipitation events.

In the present study we analyse the fall season (September, October and November; SON), and, thus 4 initialization months (May, June, July, August) which span over the SON months are used. This yields 100 seasonal weather realizations for each year between 1981 and

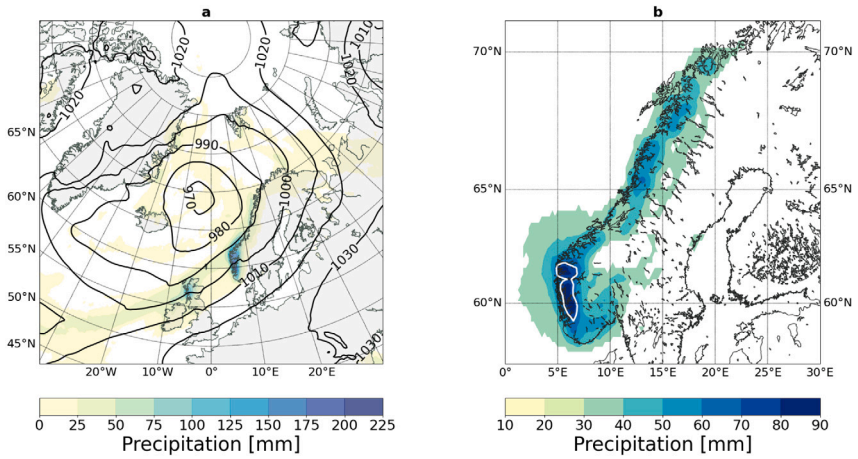

Fig. 1. **a** The synoptic situation during the extreme precipitation event 26–28 October 2014. Contours show MSLP October 26th at 12:00 UTC and precipitation values are accumulated from 26th 00:00 UTC to 29th 00:00 UTC. **b** The 98th percentile of 3-day precipitation in SON, data taken from ERA5. The white contour line indicates the chosen study region, defined by the area where the 98th percentile of the 3-day precipitation in ERA5 exceeds 70 mm.

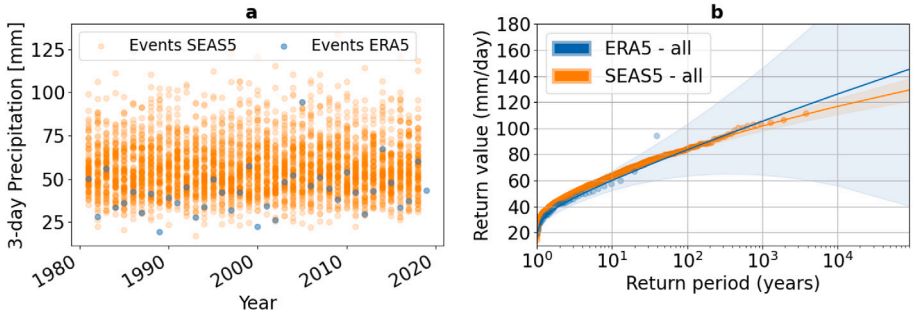

Fig. 2. **a** All seasonal max 3-day precipitation events retrieved from SEAS5 (orange dots) and equivalent from ERA5 (blue dots). **b** Generalized Extreme Value (GEV) distributions from SEAS5 (in orange) and ERA5 (in blue). Shaded areas indicate the 95% confidence interval.

2018, and in total 3800 weather realizations representing the current climate. The region of interest is located on the west coast of Norway, a region where the highest annual mean precipitation of Europe is observed and where multi-day heavy precipitation events occur frequently (Lavers and Villarini, 2015; Azad and Sorteberg, 2017). Indeed, as shown in Michel et al. (2021), this region is subject to the highest frequency of heavy precipitation events in the country, defined as the occurrences above the 99.5th percentile of the observed daily precipitation over the period 1979–2018. Further, they found the fall season being the season when most heavy precipitation events occur. As an example, one of the largest extreme precipitation events at the west coast of Norway occurred in October 2014. The synoptic atmospheric condition during this extreme precipitation event was characterized by a low pressure system located over the northern part of the Norwegian Sea, which brought warm and moist air-masses, associated with an AR, towards the west coast of Norway (Fig. 1a). Over the course of three days, the low pressure system moved slowly northeast which led to persistent precipitation in nearly the same region on the coast. This led to severe floods in several rivers with considerable damage to buildings and infrastructures.

In order to detect the extreme precipitation events in the SEAS5 hindcast data, we define our study region by using the 98th percentile of seasonal (SON) 3-day precipitation from the ERA5 reanalysis within a domain on the Norwegian south west coast for the period from 1981 to 2018 (Hersbach et al., 2018). The area where the percentile precipitation values exceed this threshold is highlighted in Fig. 1b. The area average seasonal maxima for 3-day accumulated precipitation in the selected region are combined from all relevant ensemble members and lead times in SEAS5, to construct the data-set used for the following statistical analysis. This means the data-set consists of 3800 seasonal maximum 3-day precipitation values that are fitted to a generalized extreme value (GEV) distribution to obtain return values. For comparison, we have fitted a generalized extreme value distribution to equivalent data from ERA5. The GEV-analysis is carried out applying the extRemes package in R (Gilleland and Katz, 2016).

Kelder et al. (2020) examined SEAS5 and ERA5 precipitation maxima over Norway. By comparing 3-day precipitation values with observational gridded data they concluded to apply a bias correction factor of 1.74 for precipitation in Norway. We apply the same factor here. The bias correction is a simple scaling of SEAS5 to ERA5, where we use a constant ratio between the mean of ERA5 and SEAS5 SON precipitation maxima.

The seasonal mean state of the atmosphere's circulation can be characterized by a principal component analysis of the 500 hPa geopotential anomaly for SON from the ERA5 reanalysis. The Empirical Orthogonal Function (EOF) analysis applied here was performed using the SON 500 hPa geopotential height anomalies from ERA5 and SEAS5 over the North Atlantic sector (30–88.5°N, 80°W–40°E). The 500 hPa geopotential height anomalies were weighted by the square root of the cosine of the latitude to ensure equal-area weighting before performing the analysis (Chung and Nigam, 1999). Then, the first five EOFs from ERA5 SON 500 hPa geopotential height anomalies were computed using the period from 1979 to 2017. The indices were calculated by projecting the 500 hPa geopotential heights anomalies from each SEAS5 ensemble member onto the EOFs from the ERA5 500 hPa geopotential height anomalies.

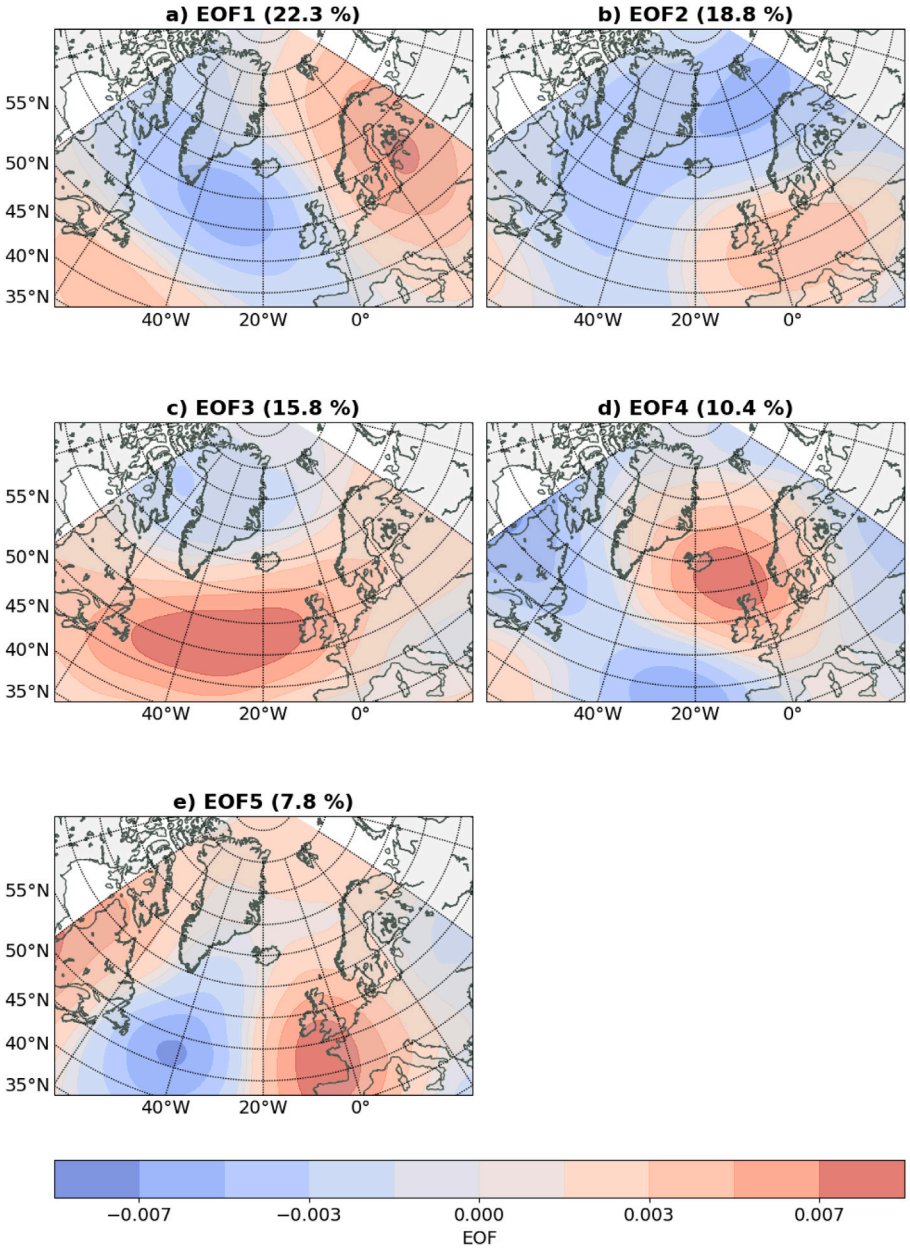

Fig. 3. The 5 first EOFs from a principal component analysis performed on the 500 hPa geopotential anomaly field for the September–October–November season. Variance explained for each EOF is given in the figure title.

The 3800 SEAS5 SON 3-day precipitation maxima now have associated seasonal indices for each of the first 5 EOFs, which can be used to analyse whether there are seasonal conditions that are connected to the extreme precipitation events. To attain this, return levels are evaluated for the different modes of EOFs for all 3800 events. Further, the main characteristics of the large-scale atmospheric setup during the extreme precipitation events in the west coast of Norway can be attained through a composite analysis of the events with the seasonal maximum 3-day precipitation in the SEAS5 data set. The SON 3-day precipitation events exceeding the 50 year return value are considered, and composite maps are made for the events according to the EOF index. The composite analysis will give the synoptic (short-term) features of different physical aspects during the extreme events. This means they will most likely not reflect the regime of the seasonal (long-term) conditions, due to atmospheric variability, but is merely used as a tool to investigate the events themselves.

3. Results

The extracted events from SEAS5 comprise a set of 3800 events, which surpass ERA5, or an observational record series from an equivalent time period, by a factor of 100. All the seasonal maximum 3-day precipitation events from SEAS5 are shown in Fig. 2a together with seasonal maximum 3-day precipitation events from ERA5. The increased sample size strongly reduces the confidence interval of the fitted distribution of extreme value statistics, as seen in Fig. 2b. For a return period of 1000 years the 95% confidence interval is ranging from 64 mm to 146 mm for data from ERA5, while for SEAS5 it is between 97 mm and 105 mm, which gives interval ranges of 82 mm and 8 mm, respectively. For a return period of 10 000 years, the confidence interval for ERA5 is −+55% of the estimated value, while for SEAS5 the interval is +−5%. In general, the confidence interval is reduced by more than a factor of 10 by using SEAS5 data compared to ERA5 data.

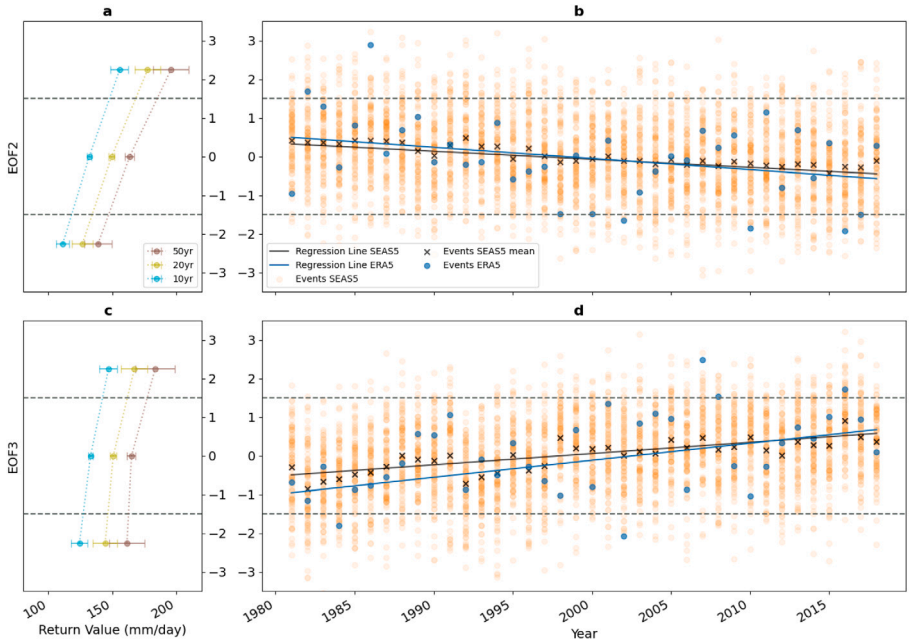

Fig. 4. The two EOFs (EOF2 top and EOF3 bottom) with the strongest connection to extreme precipitation return values. In the left panel variations in return values for return periods of 10, 20 and 50 years in the different EOF modes (positive, neutral and negative). The right panel shows the indices calculated from the EOF analysis for all events in the constructed SEAS5 data-set (orange dots) together with ERA5 data (blue dots). The black line indicates the regression line for the yearly mean of SEAS5 events (black crosses) and the blue line correspondingly for ERA5 events.

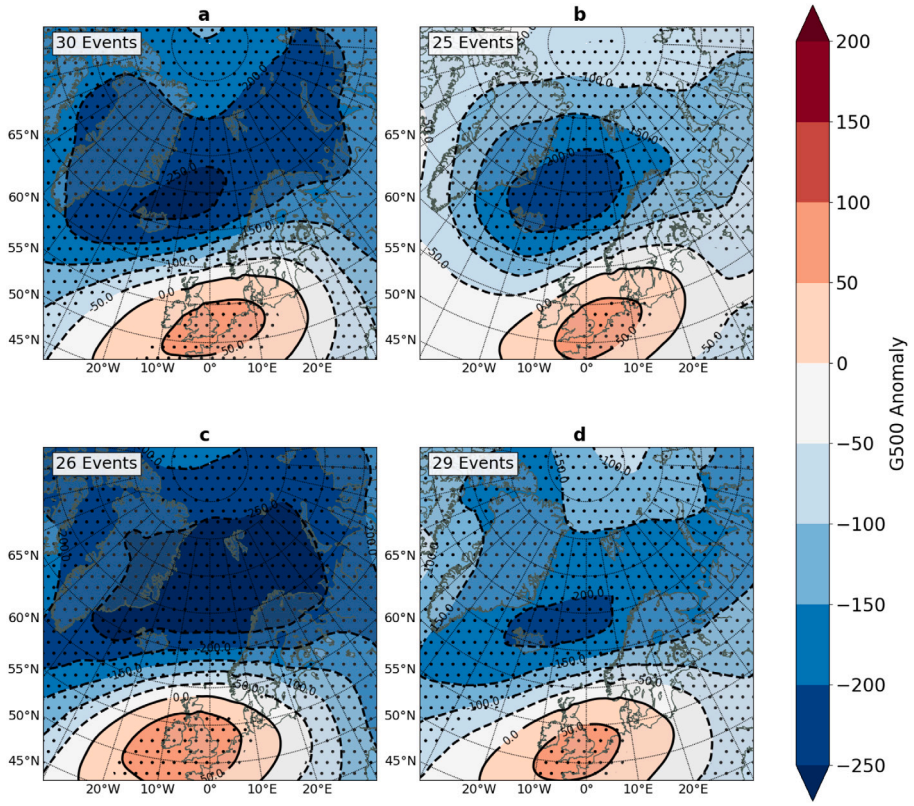

Fig. 5. Composite maps showing the geopotential height anomaly at the 500 hPa level. The anomaly is calculated relative to the season climatology, and the black dots indicate where the geopotential height anomaly is significant according to the student t-test 98% confidence, tested with False Discovery Rate approach. Composite maps in **a** and **b** show the 2nd EOF, positive and negative mode, respectively. Correspondingly in **c** and **d** for the 3rd EOF.

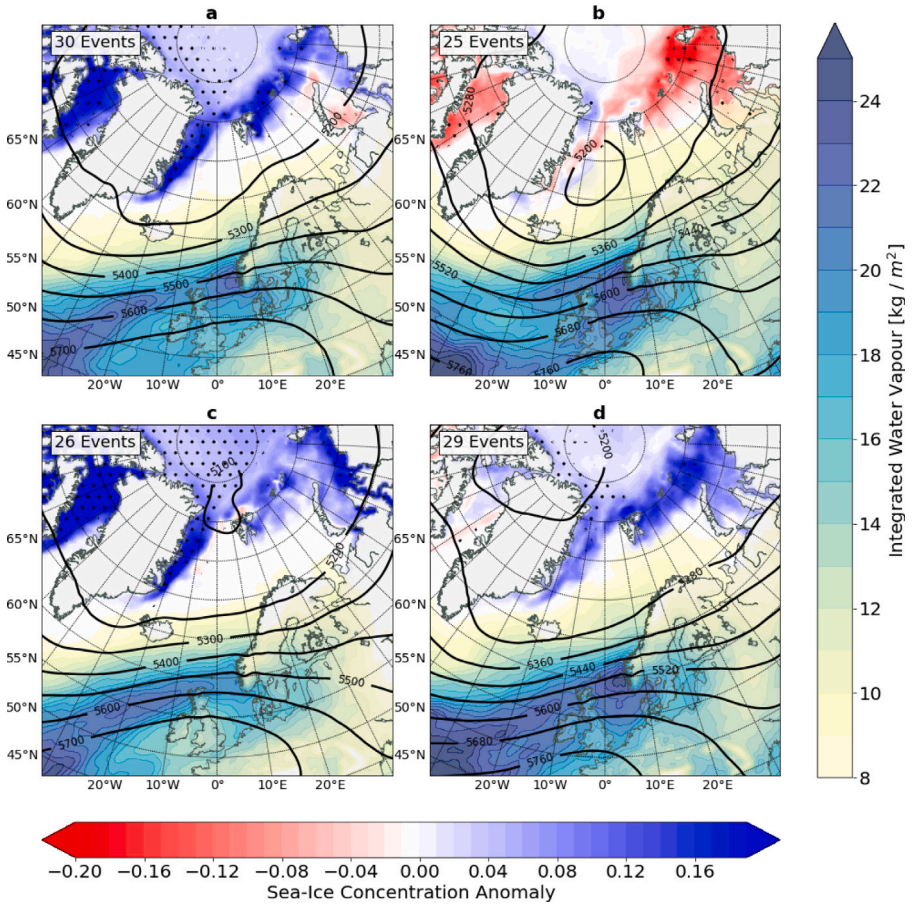

Fig. 6. Composite maps for the same events as in Fig. 5 showing sea-ice concentration anomaly calculated as the difference between the selected events and the season climatology, integrated water vapour (total column) and geopotential height at the 500 hPa level in black contours. The black dots indicate where the sea-ice concentration anomalies are significant according to the student t-test at the 95% confidence level.

The increased number of extreme events retrieved from SEAS5 opens up the possibility to analyse atmospheric properties linked to extreme events in a robust way. To identify if there are dominant circulation patterns conducive for the highest SON 3-day precipitation events in SEAS5, we are considering the first five EOFs of the 500 hPa geopotential height anomaly principal component analysis (Fig. 3). The pattern in EOF1 resembles the Scandinavian Pattern (Barnston and Livezey, 1987) which is associated with a primary circulation centre over Scandinavia and weaker centres over western Europe and eastern Russia. During the positive phase of this pattern, the geopotential height anomaly over Scandinavia is positive, which can result in a blocking system and below average precipitation across Scandinavia. The second EOF pattern has a centre of positive anomaly over western Europe and the UK and a negative anomaly field in the Arctic which stretches over Greenland and further south. It resembles the European Blocking weather regime as shown in Grams et al. (2017). There they found a positive wind speed anomaly along the coast of Norway during this regime. Further, Pasquier et al. (2019) found that this pattern allows for a more effective moisture transport around the ridge of the high pressure and into Northern Europe, with the consequence that AR frequencies are enhanced in a region extending from Iceland to Northern Scandinavia. EOF3 shows a pattern with a dipole pressure centre of positive anomaly over the Azores and negative anomaly over Iceland, which resembles the zonal regime as shown in Grams et al. (2017). The pattern has a similarity to the North Atlantic Oscillation (NAO) pattern (Barnston and Livezey, 1987; Hurrell et al., 2001), though the NAO is by definition the leading mode (1st EOF). A positive phase of this pattern is known to bring warm and wet conditions over Scandinavia (Uvo, 2003). The NAO is a leading mode of atmospheric circulation variability over the North Atlantic region. The pattern is present during the entire year, but it is more important during winter (Pinto and Raible, 2012) and relatively weak during September–October–November. The three first EOFs together explain about 57% of the variance. The positive phase of both EOF2 and EOF3 are conducive for high precipitation values over Norway by guiding low pressure systems to the west coast of the country, and are associated with higher than normal frequency of ARs (Pasquier et al., 2019).

When analysing the return values for subsets of the data corresponding to the respective values of EOF indices, we find that the second and third EOF (Fig. 3b and c) show a connection to the return values of extreme precipitation for the west coast of Norway (Fig. 4a and c). For both EOF's, using only precipitation extremes for positive EOF indices results in significantly higher return values than using events for negative EOF indices (Fig. 4a and c). Note, the sign of an EOF is ambiguous and, for the sake of simplicity, we defined the sign for EOF2 and EOF3 to positively correlate the extreme precipitation and the respective principal components.

Over the 40 year time period both EOF2 and EOF3 exhibit a trend, but with opposite signs (Fig. 4b and d). The trends were tested for significance by using the Mann–Kendall test and both trends are significant, with p-values less than 0.01, yielding a confidence level of 99%. To test the consistency with ERA5 reanalysis, the corresponding trends in EOF indices from ERA5 are included (blue dots in Fig. 4b and d). They are also significant with p-values for EOF2 and EOF3 of 0.025 and 0.0016, respectively. To test the robustness of the trends on the choice of domain for the EOF analysis, we have performed a sensitivity analysis by using five additional domains. These domains are slightly different from the original, and we perform the EOF analysis in

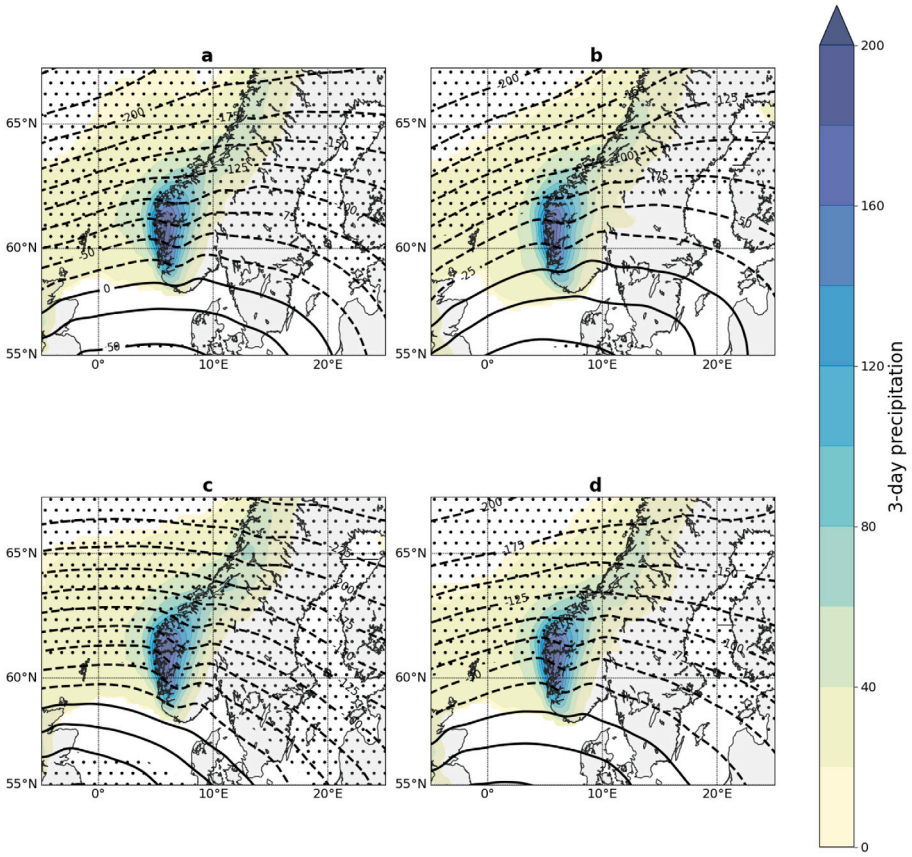

Fig. 7. Composite maps for the same events as in Fig. 6, showing the 3-day precipitation values and geopotential height anomaly at the 500 hPa level. The anomaly is calculated relative to the season climatology, and the black dots indicate where the geopotential height anomaly is significant according to the student t-test 98% confidence, tested with False Discovery Rate approach.

the same manner as the original to all five. From this we find results in agreement with the original domain, with similar trends for all the additional domains for EOF2, and for three out of five for EOF3. The results for the sensitivity analysis are summarized in Table S2 in the Supplementary Material.

Due to the difference in return values for positive and negative modes of EOF, we look closer at the precipitation events to investigate atmospheric features for events occurring during the separate modes. Composite maps can reveal characteristics of the atmospheric circulation for the selected precipitation events. Note that the pressure field during a particular event, or the composite of events, do not necessarily corresponds to the mean seasonal circulation pattern. This is due to the fact that we are considering 3-day precipitation events and the mean circulation pattern represents the whole season. We utilize only the extreme precipitation events exceeding the 50 year return value. From this subset, we further divide the events into positive and negative modes of EOF2 and EOF3 for the composites (Figs. 5 and 6). The 500 hPa geopotential anomaly composites show a dipole structure with negative anomaly situated over the Greenland and Norwegian Seas and a positive anomaly centre located over the UK and West Europe. The main difference between the patterns is seen in the extent and strength of the negative anomaly and the location of the high anomaly centre and zero-anomaly line. For the figures with positive EOF indices (Figs. 5 and 6a and c), the negative anomaly is not only deeper, but has a larger extent than for the figures showing negative EOF indices (Figs. 5 and 6b and d). The more negative geopotential height anomalies for the positive modes of the EOFs will cause stronger pressure gradients that leads to stronger flows towards the west coast, where the flow will be lifted orographically and lead to heavier precipitation.

Over the years from 1981 to 2018 EOF2 has had a negative trend, towards the indices that are associated with lower return values. The maps in Figs. 5b and 6b are the composite of events with lowest indices of EOF2, thus the composite of events which are more frequently occurring in the most recent years in the data-set. This composite map stands out from the rest, as the area with negative height anomaly is more confined than in Figs. 5 and 6a, c and d. Another notable feature in Fig. 6b is the sea-ice extent in the Barents-Kara Sea, which is smaller here compared to what is seen in Fig. 6a, c and d. Sea-ice concentration has had a decreasing trend in recent decades, and the minimum annual sea-ice extents in 2020 and 2019 are the second and third lowest on record. Sea-ice extent can influence the energy budget in the Arctic, and is connected to atmospheric circulation patterns (Vihma, 2014). Figure S1 (in the Supplementary Material) shows the SST anomaly for the same events as in Fig. 6. Although it is not significant, there is a signal of the events in Fig. 6b having higher SST values than the rest, concurrent with the events that had the lowest sea-ice extent. These are the events composed by low indices of EOF2, and given the trend found in Fig. 4b implies conditions that lead to precipitation events with lower return values on the west coast of Norway in the autumn season.

Comparing the composites of events occurring during positive and negative indices for the two EOFs, a difference in the pressure gradient can be seen in Fig. 7, where the geopotential height anomaly lines are closer in Fig. 7a and c (positive indices) compared to Fig. 7b and d (negative indices). The trend in EOF2 is thus towards events with more frequently occurring circulation with weaker pressure gradient. The weaker pressure gradient implies a weaker flow, resulting in lower precipitation amounts over the west coast of Norway. In contrast, the trend in EOF3 implies events with more frequently occurring circulation characterized by a stronger pressure gradient. This is conducive for a stronger flow, which results in precipitation events associated with higher return values.

4. Discussion and conclusions

The characteristics of extreme precipitation are expected to change drastically in our warming climate (Myhre et al., 2019). The west coast of Norway, and especially the south west coast, is subject to the largest rainfall amounts in Norway, with an annual mean precipitation exceeding 3000 mm (Lussana et al., 2018). In order to investigate the recent changes of extreme precipitation along the west coast of Norway, we are using a large ensemble generated from the SEAS5 seasonal hindcast data-set which represents the climate from 1981 to 2018 (Johnson et al., 2019). From this data-set 3800 annual 3-day precipitation maxima are extracted for the SON season and for a region on the west coast of Norway. The extreme precipitation events are analysed by means of the GEV distribution and by the preconditioning mean seasonal atmospheric patterns using EOF analysis.

The large data set offers an increased precipitation event sample size that strongly reduces the uncertainty in design value estimates. The confidence interval is reduced by more than a factor of 10 when SEAS5 events are used in a fit to the GEV distribution compared to using data from ERA5. Design values are frequently used estimates when planning and designing public buildings or communication structures, and reliable information is crucial for raising and maintaining robust infrastructures. The complex topography in Norway gives rise to large heterogeneities in precipitation extremes for different parts of the country, and limitations in observational records makes design value estimation challenging. This methodology gives the opportunity to reduce uncertainties in areas where already existing design value estimates are based on sparse observations or time limited reanalysis data-sets, and it especially strengthens the estimates for long return periods.

In addition to a more robust extreme value distribution statistics, the increased sample size allows for a more robust analysis of atmospheric properties connected to extreme events. If there are persistent and reoccurring weather patterns during a season, the seasonal mean atmospheric state will be influenced and predominated by this. For this reason, seasonal EOF indices are used to investigate whether there are conditions that are favourable for extremes during a season. We find that the return periods and return values of extreme precipitation are related to two EOF atmospheric circulation modes. The two EOFs are patterns favourable for higher precipitation amounts on the west coast of Norway and thus are also related to the probability of occurrence of extreme events: the pattern of EOF2 is associated with higher than normal air flow along the coast of Norway, which is also coupled with a more effective moisture transport into Northern Europe and enhanced AR frequencies (Pasquier et al., 2019), and the more zonal regime in EOF3 is associated with warm and wet conditions over Scandinavia (Uvo, 2003). The principal components of two EOFs exhibit significant trends over the 40 year time period, however, with an opposing impact on the extreme precipitation. In total, this leads to a virtually non-changing extreme precipitation over the west coast of Norway over the past 40 years.

Our results are consistent with Kelder et al. (2020), who analysed variability in precipitation in autumn in a similar region at the west coast of Norway and found no trend in extreme precipitation for this period. From a climate model analysis Whan et al. (2020) found that there is only little change from the past (around 1850) to the near-future periods (around 2030) in the number of Atmospheric Rivers reaching the west-coast of Norway and the extreme precipitation. However, drastic increases are found for the far-future (around 2100). Other studies on the recent changes in mean precipitation from observation records show increasing precipitation amounts for Norway, and climate predictions expect further increase in the years to come (Hanssen-Bauer et al., 2017). The annual total has had an increasing trend, with an exception for the autumn season (Kuya et al., 2021).

Circulation patterns are driven by the Earth's energy balance and are controlled by complex interactions within the coupled Earth–Atmosphere system. They are thus subject to the currently changing climate. In order to better understand the interconnected changes in the coupled ocean–ice–atmospheric system we combined the analysis of the geopotential height fields, sea-ice extent, and SST for the largest extreme events (exceeding 50 year return value) and, further, sub-divided them into the predominant EOF conditions. We have found an inherent connection of the ocean surface temperatures and sea-ice coverage in the Barents-Kara Sea for EOF2. In other words, extreme precipitation events which occur in seasons where the mean atmospheric state is dominated by a positive (negative) EOF2 atmospheric pattern are also occurring during positive (negative) anomalies of sea-ice in the Euro Atlantic sector, as well as negative (positive) ocean surface temperature anomalies.

There are a number of studies on linkages between sea-ice, ocean surface temperatures and mid-latitude weather patterns (e.g. Magnusdottir et al. (2004), Vihma (2014), Tokinaga et al. (2017)). On the one hand, SST is an important driver in planetary-scale atmospheric circulation which can again transport warm air into the Arctic and contribute to sea-ice loss (Tokinaga et al., 2017). In particular, the variability of the SST in the Gulf Stream area is potentially linked to an upper-tropospheric wave response which causes atmospheric patterns over the North Atlantic with predominant southerly winds (Sato et al., 2014), with a subsequent impact on the sea-ice coverage of the Barents-Kara Sea (Nakanowatari et al., 2014).

On the other hand, sea-ice variability for example in the Barents-Kara Sea region might have important implications on the state of the atmosphere. For example Ruggieri et al. (2016) describe a mechanism which causes an atmospheric blocking like signal over the Barents-Kara Sea region during low sea-ice conditions. Hence, the statistical correlation of SST and sea-ice variability to the extreme precipitation in relation to EOF2 suggests that this change might be connected to our warming climate. However, a more detailed study on the different Earth's system components will be necessary to disentangle the processes.

In our study, EOF3 shows a north–south dipole structure with negative pressure anomaly over Iceland and positive pressure anomaly over the Azores, thus a zonal regime that is similar to the NAO pattern. The detected change in EOF3 might be associated with a region south of Greenland with a slower warming rate than the North Atlantic Ocean in general (Rahmstorf et al., 2015), which causes a local increase of the north–south temperature gradient over the ocean surface (Harvey and Shaffrey, 2021), which again influences the pressure gradient. In isolation this trend in EOF3 leads to increasing precipitation with higher return values at the west coast of Norway. This impact is diminished by the trend in the 2nd EOF and its opposing effect on extreme precipitation.

We find two seasonal atmospheric patterns which have a connection to the extreme precipitation, but the patterns themselves have an opposing trend. Choosing different areas for the EOF analysis might remove this separation and one thus could argue that this is an artificial separation into these two patterns by the EOF method. However, for the two patterns we also find different correlations to the sea-ice extent, which supports the fact that the separation is meaningful.

The novel extreme event analysis approach presented here has proven to be useful for studying the relation of extreme precipitation with other dynamical components. The method reduces uncertainties in statistical analysis due to the increased sample size, and allows to find connections between the extreme precipitation events and atmospheric circulation patterns, sea-ice variability, or ocean-surface conditions. A natural next step would be to investigate the mechanisms causing this relationship, which can improve our understanding of the driving forces for extreme precipitation events.

CRediT authorship contribution statement

Karianne Ødemark: Conception and design of study, Acquisition of data, Analysis and/or interpretation of data, Writing – original draft. **Malte Müller:** Conception and design of study, Acquisition of data, Analysis and/or interpretation of data, Writing – review & editing. **Cyril Palerme:** Acquisition of data, Analysis and/or interpretation of data. **Ole Einar Tveito:** Analysis and/or interpretation of data, Writing – review & editing.

Declaration of competing interest

The authors declare that they have no known competing financial interests or personal relationships that could have appeared to influence the work reported in this paper.

Data availability

Data will be made available on request.

Acknowledgements

The study is supported by the Norwegian Research Council and Energi Norge, Norway through the project FlomQ (NFR-235710/E20). MM has received support from the project TWEX (NFR-255037) funded through the Norwegian Research Council. The data from SEAS5 and ERA5 data are available from the Copernicus Climate Change Service (C3S) Climate DataStore (https://cds.climate.copernicus.eu/). The authors would like to thank the editor and two reviewers for their help in improving the paper. We are also thankful for helpful input from Inger Hanssen-Bauer. All authors approved the version of the manuscript to be published.

Appendix A. Supplementary data

Supplementary material related to this article can be found online at https://doi.org/10.1016/j.wace.2022.100530.

References

Azad, R., Sorteberg, A., 2017. Extreme daily precipitation in coastal western Norway and the link to atmospheric rivers. J. Geophys. Res.: Atmos. 122 (4), 2080–2095. http://dx.doi.org/10.1002/2016JD025615, arXiv:https://agupubs.onlinelibrary.wiley.com/doi/pdf/10.1002/2016JD025615, URL https://agupubs.onlinelibrary.wiley.com/doi/abs/10.1002/2016JD025615.

Barnston, A.G., Livezey, R.E., 1987. Classification, Seasonality and Persistence of Low-Frequency Atmospheric Circulation Patterns. Mon. Weather Rev. 115 (6), 1083–1126. http://dx.doi.org/10.1175/1520-0493(1987)115<1083:CSAPOL>2.0.CO;2, URL https://journals.ametsoc.org/view/journals/mwre/115/6/1520-0493_1987_115_1083_csapol_2_0_co_2.xml.

Benedict, I., Ødemark, K., Nipen, T., Moore, R., 2019. Large-Scale Flow Patterns Associated with Extreme Precipitation and Atmospheric Rivers over Norway. Mon. Weather Rev. 147 (4), 1415–1428. http://dx.doi.org/10.1175/MWR-D-18-0362.1.

Bintanja, R., van der Wiel, K., van der Linden, E.C., Reusen, J., Bogerd, L., Krikken, F., Selten, F.M., 2020. Strong future increases in Arctic precipitation variability linked to poleward moisture transport. Sci. Adv. 6 (7), http://dx.doi.org/10.1126/sciadv.aax6869, arXiv:https://advances.sciencemag.org/content/6/7/eaax6869.full.pdf, URL https://advances.sciencemag.org/content/6/7/eaax6869.

Blackport, R., Screen, J.A., van der Wiel, K., Bintanja, R., 2019. Minimal influence of reduced Arctic sea ice on coincident cold winters in mid-latitudes. Nature Clim. Change 9, http://dx.doi.org/10.1038/s41558-019-0551-4.

Boucher, O., Randall, D., Artaxo, P., Bretherton, C., Feingold, G., Forster, P., Kerminen, V.-M., Kondo, Y., Liao, H., Lohmann, U., Rasch, P., Satheesh, S.K., Sherwood, S., Stevens, B., Zhang, X.Y., 2013. Clouds and aerosols. In: Stocker, T.F., Qin, D., Plattner, G.-K., Tignor, M., Allen, S.K., Doschung, J., Nauels, A., Xia, Y., Bex, V., Midgley, P.M. (Eds.), Climate Change 2013: The Physical Science Basis. Contribution of Working Group I To the Fifth Assessment Report of the Intergovernmental Panel on Climate Change. Cambridge University Press, Cambridge, UK, pp. 571–657. http://dx.doi.org/10.1017/CBO9781107415324.016.

Chung, C., Nigam, S., 1999. Weighting of geophysical data in Principal Component Analysis. J. Geophys. Res.: Atmos. 104, http://dx.doi.org/10.1029/1999JD900234.

Coumou, D., Petoukhov, V., Rahmstorf, S., Petri, S., Schellnhuber, H.J., 2014. Quasi-resonant circulation regimes and hemispheric synchronization of extreme weather in boreal summer. Proc. Natl. Acad. Sci. USA 111, http://dx.doi.org/10.1073/pnas.1412797111.

Dee, D.P., Uppala, S.M., Simmons, A.J., Berrisford, P., Poli, P., Kobayashi, S., Andrae, U., Balmaseda, M.A., Balsamo, G., Bauer, P., Bechtold, P., Beljaars, A.C.M., van de Berg, L., Bidlot, J., Bormann, N., Delsol, C., Dragani, R., Fuentes, M., Geer, A.J., Haimberger, L., Healy, S.B., Hersbach, H., Hólm, E.V., Isaksen, L., Kållberg, P., Köhler, M., Matricardi, M., McNally, A.P., Monge-Sanz, B.M., Morcrette, J.-J., Park, B.-K., Peubey, C., de Rosnay, P., Tavolato, C., Thépaut, J.-N., Vitart, F., 2011. The ERA-Interim reanalysis: configuration and performance of the data assimilation system. Q. J. R. Meteorol. Soc. 137, 553–597. http://dx.doi.org/10.1002/qj.828, URL https://rmets.onlinelibrary.wiley.com/doi/abs/10.1002/qj.828.

ECMWF, 2016. IFS documentation CY43R1. http://dx.doi.org/10.21957/m1u2yxwrl, URL https://www.ecmwf.int/node/17116.

Eyring, V., Bony, S., Meehl, G.A., Senior, C.A., Stevens, B., Stouffer, R.J., Taylor, K.E., 2016. Overview of the Coupled Model Intercomparison Project Phase 6 (CMIP6) experimental design and organization. Geosci. Model Dev. 9, http://dx.doi.org/10.5194/gmd-9-1937-2016.

Fichefet, T., Maqueda, M.A.M., 1997. Sensitivity of a global sea ice model to the treatment of ice thermodynamics and dynamics. J. Geophys. Res.: Oceans 102 (C6), 12609–12646. http://dx.doi.org/10.1029/97JC00480, arXiv:https://agupubs.onlinelibrary.wiley.com/doi/pdf/10.1029/97JC00480, URL https://agupubs.onlinelibrary.wiley.com/doi/abs/10.1029/97JC00480.

Fischer, E.M., Knutti, R., 2016. Observed heavy precipitation increase confirms theory and early models. Nature Clim. Change 6, http://dx.doi.org/10.1038/nclimate3110.

Francis, J.A., Vavrus, S.J., 2012. Evidence linking Arctic amplification to extreme weather in mid-latitudes. Geophys. Res. Lett. 39, http://dx.doi.org/10.1029/2012GL051000.

Gilleland, E., Katz, R., 2016. Extremes 2.0: An Extreme Value Analysis Package in R. J. Stat. Softw. Articles 72, 1–39. http://dx.doi.org/10.18637/jss.v072.i08, URL https://www.jstatsoft.org/v072/i08.

Gimeno, L., Nieto, R., Vázquez, M., Lavers, D.A., 2014. Atmospheric rivers: A mini-review. Front. Earth Sci. 2, http://dx.doi.org/10.3389/feart.2014.00002.

Grams, C.M., Beerli, R., Pfenninger, S., Staffell, I., Wernli, H., 2017. Balancing Europe's wind-power output through spatial deployment informed by weather regimes. Nature Clim. Change 7, 557–562. http://dx.doi.org/10.1038/NCLIMATE3338.

Hanssen-Bauer, I., Førland, E., Haddeland, I., Hisdal, H., Lawrence, D., Mayer, S., Nesje, A., Nilsen, J., Sandven, S., Sandø, A., Sorteberg, A., Ådlandsvik, B., 2017. Climate in Norway 2100 - a knowledge base for climate adaption.

Harvey, B., Shaffrey, L., 2021. How will climate change impact North Atlantic storms? Weather 76, http://dx.doi.org/10.1002/wea.4075.

Hersbach, H., de Rosnay, P., Bell, B., Schepers, D., Simmons, A., Soci, C., Abdalla, S., Alonso-Balmaseda, M., Balsamo, G., Bechtold, P., Berrisford, P., Bidlot, J.-R., de Boisséson, E., Bonavita, M., Browne, P., Buizza, R., Dahlgren, P., Dee, D., Dragani, R., Diamantakis, M., Flemming, J., Forbes, R., Geer, A.J., Haiden, T., Hólm, E., Haimberger, L., Hogan, R., Horányi, A., Janiskova, M., Laloyaux, P., Lopez, P., Munoz-Sabater, J., Peubey, C., Radu, R., Richardson, D., Thépaut, J.-N., Vitart, F., Yang, X., Zsótér, E., Zuo, H., 2018. Operational global reanalysis: progress, future directions and synergies with NWP. ERA Rep. Series http://dx.doi.org/10.21957/tkic6g3wm, URL https://www.ecmwf.int/node/18765.

Horton, D.E., Johnson, N.C., Singh, D., Swain, D.L., Rajaratnam, B., Diffenbaugh, N.S., 2015. Contribution of changes in atmospheric circulation patterns to extreme temperature trends. Nature 522, http://dx.doi.org/10.1038/nature14550.

Hurrell, J.W., Kushnir, Y., Visbeck, M., 2001. The North Atlantic oscillation. Science 291, http://dx.doi.org/10.1126/science.1058761.

Johnson, S.J., Stockdale, T.N., Ferranti, L., Balmaseda, M.A., Molteni, F., Magnusson, L., Tietsche, S., Decremer, D., Weisheimer, A., Balsamo, G., Keeley, S.P., Mogensen, K., Zuo, H., Monge-Sanz, B.M., 2019. SEAS5: The new ECMWF seasonal forecast system. Geosci. Model Dev. 12, http://dx.doi.org/10.5194/gmd-12-1087-2019.

Kelder, T., Müller, M., Slater, L.J., Marjoribanks, T.I., Wilby, R.L., Prudhomme, C., Bohlinger, P., Ferranti, L., Nipen, T., 2020. Using UNSEEN trends to detect decadal changes in 100-year precipitation extremes. Npj Climate Atmospheric Sci. 3, http://dx.doi.org/10.1038/s41612-020-00149-4.

Kharin, V.V., Zwiers, F.W., Zhang, X., Wehner, M., 2013. Changes in temperature and precipitation extremes in the CMIP5 ensemble. Clim. Change 119, http://dx.doi.org/10.1007/s10584-013-0705-8.

Kolstad, E.W., Screen, J.A., 2019. Nonstationary Relationship Between Autumn Arctic Sea Ice and the Winter North Atlantic Oscillation. Geophys. Res. Lett. 46, 7583–7591. http://dx.doi.org/10.1029/2019GL083059.

Kuya, E.K., Gjelten, H.M., Tveito, O.E., 2021. Homogenization of Norwegian monthly precipitation series for the period 1961–2018. URL https://www.met.no/publikasjoner/met-report.

Lavers, D.A., Villarini, G., 2015. The contribution of atmospheric rivers to precipitation in Europe and the United States. J. Hydrol. 522, http://dx.doi.org/10.1016/j.jhydrol.2014.12.010.

Lussana, C., Saloranta, T., Skaugen, T., Magnusson, J., Tveito, O.E., Andersen, J., 2018. seNorge2 daily precipitation, an observational gridded dataset over Norway from 1957 to the present day. Earth Syst. Sci. Data 10, 235–249. http://dx.doi.org/10.5194/essd-10-235-2018, URL https://www.earth-syst-sci-data.net/10/235/2018/.

Madec, G., Bourdallé-Badie, R., Bouttier, P.-A., Bricaud, C., Bruciaferri, D., Calvert, D., Chanut, J., Clementi, E., Coward, A., Delrosso, D., Ethé, C., Flavoni, S., Graham, T., Harle, J., Iovino, D., Lea, D., Lévy, C., Lovato, T., Martin, N., Masson, S., Mocavero, S., Paul, J., Rousset, C., Storkey, D., Storto, A., Vancoppenolle, M., 2017. NEMO ocean engine. URL http://hdl.handle.net/2122/13309.

Magnusdottir, G., Deser, C., Saravanan, R., 2004. The effects of North Atlantic SST and sea ice anomalies on the winter circulation in CCM3. Part I: Main features and storm track characteristics of the response. J. Clim. 17, http://dx.doi.org/10.1175/1520-0442(2004)017<0857:TEONAS>2.0.CO;2.

Michel, C., Sorteberg, A., Eckhardt, S., Weijenborg, C., Stohl, A., Cassiani, M., 2021. Characterization of the atmospheric environment during extreme precipitation events associated with atmospheric rivers in Norway - Seasonal and regional aspects. Weather Climate Extremes 34, http://dx.doi.org/10.1016/j.wace.2021.100370.

Myhre, G., Alterskjær, K., Stjern, C.W., Hodnebrog, Marelle, L., Samset, B.H., Sillmann, J., Schaller, N., Fischer, E., Schulz, M., Stohl, A., 2019. Frequency of extreme precipitation increases extensively with event rareness under global warming. Sci. Rep. 9, http://dx.doi.org/10.1038/s41598-019-52277-4.

Nakanowatari, T., Sato, K., Inoue, J., 2014. Predictability of the Barents sea ice in early winter: Remote effects of oceanic and atmospheric thermal conditions from the North Atlantic. J. Clim. 27, http://dx.doi.org/10.1175/JCLI-D-14-00125.1.

Ødemark, K., Müller, M., Tveito, O.E., 2020. Changing lateral boundary conditions for probable maximum precipitation studies: A physically consistent approach. J. Hydrometeorol. 22, http://dx.doi.org/10.1175/JHM-D-20-0070.1.

Papalexiou, S.M., Montanari, A., 2019. Global and Regional Increase of Precipitation Extremes Under Global Warming. Water Resour. Res. 55, http://dx.doi.org/10.1029/2018WR024067.

Pasquier, J.T., Pfahl, S., Grams, C.M., 2019. Modulation of Atmospheric River Occurrence and Associated Precipitation Extremes in the North Atlantic Region by European Weather Regimes. Geophys. Res. Lett. 46, http://dx.doi.org/10.1029/2018GL081194.

Pinto, J.G., Raible, C.C., 2012. Past and recent changes in the North Atlantic oscillation. Wiley Interdiscip. Rev. Clim. Change 3, 79–90. http://dx.doi.org/10.1002/wcc.150.

Rahmstorf, S., Box, J.E., Feulner, G., Mann, M.E., Robinson, A., Rutherford, S., Schaffernicht, E.J., 2015. Exceptional twentieth-century slowdown in Atlantic Ocean overturning circulation. Nature Clim. Change 5, http://dx.doi.org/10.1038/nclimate2554.

Ruggieri, P., Buizza, R., Visconti, G., 2016. On the link between Barents-Kara sea ice variability and European blocking. J. Geophys. Res. 121, 5664–5679. http://dx.doi.org/10.1002/2015JD024021.

Sato, K., Inoue, J., Watanabe, M., 2014. Influence of the Gulf Stream on the Barents Sea ice retreat and Eurasian coldness during early winter. Environ. Res. Lett. 9, http://dx.doi.org/10.1088/1748-9326/9/8/084009.

Screen, J.A., 2017. Simulated Atmospheric Response to Regional and Pan-Arctic Sea Ice Loss. J. Clim. 30, 3945–3962. http://dx.doi.org/10.1175/JCLI-D-16-0197.1.

Serreze, M.C., Barry, R.G., 2011. Processes and impacts of Arctic amplification: A research synthesis. Glob. Planet. Change 77 (1), 85–96. http://dx.doi.org/10.1016/j.gloplacha.2011.03.004, URL https://www.sciencedirect.com/science/article/pii/S0921818111000397.

Smith, D.M., Eade, R., Andrews, M.B., Ayres, H., Clark, A., Deser, C., Dunstone, N.J., García-Serrano, J., Gastineau, G., Graff, L.S., Hardiman, S.C., He, B., Hermanson, L., Jung, T., Knight, J., Levine, X., Magnusdottir, G., Manzini, E., Matei, D., Mori, M., Msadek, R., Ortega, P., Peings, Y., Scaife, A.A., Screen, J.A., Seabrook, M., Semmler, T., Sigmond, M., Streffing, J., Sun, L., Walsh, A., 2022. Robust but weak winter atmospheric circulation response to future Arctic sea ice loss. Nature Commun. 13, http://dx.doi.org/10.1038/s41467-022-28283-y.

Smith, D.M., Screen, J.A., Deser, C., Cohen, J., Fyfe, J.C., García-Serrano, J., Jung, T., Kattsov, V., Matei, D., Msadek, R., Peings, Y., Sigmond, M., Ukita, J., Zhang, X., 2019. The Polar Amplification Model Intercomparison Project (PAMIP) contribution to CMIP6: Investigating the causes and consequences of polar amplification. Geosci. Model Dev. 12, http://dx.doi.org/10.5194/gmd-12-1139-2019.

Sodemann, H., Stohl, A., 2013. Moisture Origin and Meridional Transport in Atmospheric Rivers and Their Association with Multiple Cyclones. Mon. Wea. Rev. 141 (8), 2850–2868.

Stohl, A., Forster, C., Sodemann, H., 2008. Remote sources of water vapor forming precipitation on the Norwegian west coast at 60°N–a tale of hurricanes and an atmospheric river. J. Geophys. Res.: Atmos. 113 (D5), n/a–n/a. http://dx.doi.org/10.1029/2007JD009006, D05102.

Sun, L., Deser, C., Tomas, R.A., 2015. Mechanisms of stratospheric and tropospheric circulation response to projected Arctic sea ice loss. J. Climate 28, 7824–7845.

Tamarin-Brodsky, T., Kaspi, Y., 2017. Enhanced poleward propagation of storms under climate change. Nat. Geosci. 10, http://dx.doi.org/10.1038/s41561-017-0001-8.

Tokinaga, H., Xie, S.P., Mukougawa, H., 2017. Early 20th-century Arctic warming intensified by Pacific and Atlantic multidecadal variability. Proc. Natl. Acad. Sci. USA 114, http://dx.doi.org/10.1073/pnas.1615880114.

Uvo, C.B., 2003. Analysis and regionalization of northern European winter precipitation based on its relationship with the North Atlantic Oscillation. Int. J. Climatol. 23 (10), 1185–1194.

Vihma, T., 2014. Effects of Arctic Sea Ice Decline on Weather and Climate: A review. Surv. Geophys. 35, 1175–1214. http://dx.doi.org/10.1007/s10712-014-9284-0.

Whan, K., Sillmann, J., Schaller, N., Haarsma, R., 2020. Future changes in atmospheric rivers and extreme precipitation in Norway. Clim. Dynam. 54, http://dx.doi.org/10.1007/s00382-019-05099-z.

Wickström, S., Jonassen, M.O., Vihma, T., Uotila, P., 2020. Trends in cyclones in the high-latitude North Atlantic during 1979–2016. Q. J. R. Meteorol. Soc. 146, http://dx.doi.org/10.1002/qj.3707.

Zhu, Y., Newell, R.E., 1998. A proposed algorithm for moisture fluxes from atmospheric rivers. Mon. Weather Rev. 126, http://dx.doi.org/10.1175/1520-0493(1998)126<0725:APAFMF>2.0.CO;2.

Zuo, H., Alonso-Balmaseda, M., Mogensen, K., Tietsche, S., 2018. OCEAN5: The ECMWF ocean reanalysis system and its real-time analysis component. http://dx.doi.org/10.21957/la2v0442, URL https://www.ecmwf.int/node/18519.